Giant Change in Electrical Resistivity Induced by Moderate Pressure in Pt(bqd)2 – First Candidate Material for an Organic Piezoelectronic Transistor (OPET)

ADVANCED ELECTRONIC MATERIALS Open Access
www.advelectronicmat.de

Giant Change in Electrical Resistivity Induced by Moderate Pressure in Pt(bqd)2 – First Candidate Material for an Organic Piezoelectronic Transistor (OPET)

Sergejs Afanasjevs, Helen Benjamin, Konstantin Kamenev, and Neil Robertson*

The piezoelectronic transistor (PET) has been proposed to overcome the voltage and clock speed limitations of conventional field-effect transistors (FET). In a PET, voltage is transduced to stress, which leads to an insulator-metal transition in a piezo-resistive (PR) element. Although the simulated switching speeds are promising, the viable candidates proposed so far for the PR layer are rare earth compounds that require several GPa of pressure (*P*) to metalize, necessitating breakthroughs in transduction mechanism scaling and processing. Here, a PR candidate that metalizes in the 0–300 MPa range – the transition metal complex platinum benzoquinonedioximato ($Pt(bqd)_2$) is demonstrated. Such electrical sensitivity to the application of *P* arises when the material is grown as a thin film with the preferred needle orientation perpendicular to the substrate. As evidence, a combination of hydrostatic and uniaxial pressure studies is provided. The former studies are produced on the compressed powder pellet in a specially developed piston-cylinder cell (P-C cell) under variable temperatures (*T*) and *P*. The latter is via thin film deposition and uniaxial resistivity (ρ) measurements and these revealed the high potential of this material for the PET concept.

1. Introduction

The rapid increase in computing power has been illustrated by two factors: i) "Moore's law"- which states that the number of transistors on processors should double roughly every 18 months, and ii) the associated increase in clock speed brought about by increased transistor density. While the former factor remains true and transistor densities continue to increase, the latter has stalled due to the operating principle of filed-effect transistors (FETs). There is a minimum gate voltage required to switch the transistor from an "Off" state to an "On" state, determined by the thermal excitation of charge carriers in the "Off" state of the device, which does not scale with the device dimension. The practical lower limit for the gate voltage required to achieve an "On-Off" resistivity (ρ) ratio of $\approx 10^4$ is $\approx$1 V; this was achieved in 2004.[1] Additionally, as the size of devices is further reduced, leakage currents in the "Off" state also become an issue. As a result, there have been no further clock speed increases in central processing units (CPUs), frequencies of which can barely reach 6 GHz when boosted and professionally cooled (Figure S1, Supporting Information).

To overcome the fundamental limitations of FET and to restore Dennard's scaling, International Business Machines Corporation (IBM) proposed a new transistor concept that provides both low voltage/power and high-frequency operation – Piezoelectronic Transistor (PET) (**Figure 1**).[2,3,12]

When Voltage (*V*) is applied at Gate, piezoelectric (PE) material expands and uniaxially compresses piezoresistive (PR) material which undergoes insulator to metal transition allowing current to pass from Common to Sense within high-yield material (HYM).

PET utilizes piezoelectric actuation to propagate digital logic, and early simulations promise a 10 GHz frequency at 150 mV with further performance increases at reduced scales.[3] However, the candidates for the PR layer so far proposed and tested by IBM are rare earth compounds such as SmSe, TmTe, and $Sm_xEu_{1-x}S$, that require several GPa of pressure (*P*) to metalize, necessitating breakthroughs in piezoelectric actuator scaling and processing, and provide little opportunity for synthetic modification.[4]

Organic materials show a tremendous diversity of electrical conductivity (σ) behavior and have been found to exist as semiconductors,[5] metals[6] and superconductors.[7]

S. Afanasjevs, K. Kamenev
Centre for Science at Extreme Conditions
School of Engineering
The University of Edinburgh
Edinburgh EH8 9YL, UK
E-mail: safanas2@ed.ac.uk
H. Benjamin, N. Robertson
Eastchem School of Chemistry
The University of Edinburgh
Edinburgh UK
H. Benjamin
Cambridge Display Technology Ltd.
Unit 12 Cardinal Park, Cardinal Way, Godmanchester, Cambridgeshire UK
The ORCID identification number(s) for the author(s) of this article can be found under https://doi.org/10.1002/aelm.202300680

DOI: 10.1002/aelm.202300680

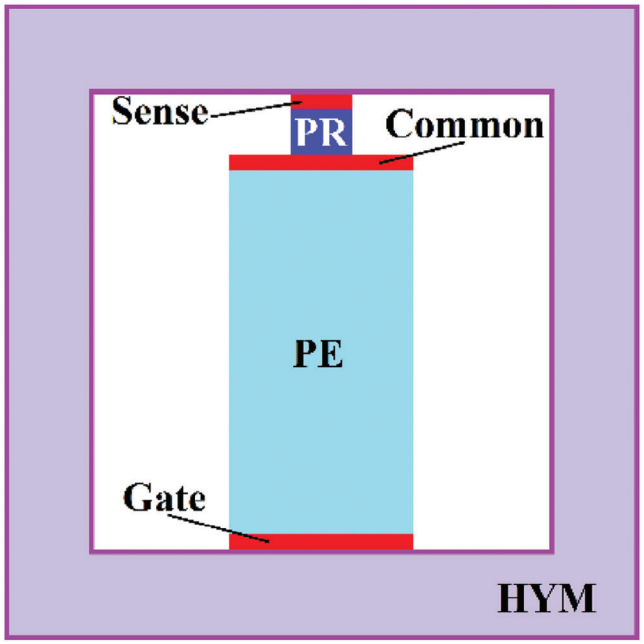

Figure 1. Schematic of PET structure.

Because of their layered crystal structure, these materials exhibit anisotropic properties. In combination with relatively weak Van Der Waals interactions between the molecules, these result in highly anisotropic compressibility of the materials, often at relatively low *P*, making them suitable candidates for PET.

One such material is platinum benzoquinonedioximato ($Pt(bqd)_2$) (**Figure 2**), which belongs to the square planar d^8 complexes, known to have a propensity to form one-dimensional stacking with short metal-metal distances.[8] This, in turn, presumes higher conductive properties under extremes of *P*; the ρ of $Pt(bqd)_2$ decreases by 4–5 orders of magnitude under an applied *P* of only 1.5 GPa.[9]

In our previous work,[10] we have successfully investigated the structural and electronic property response of $Pt(bqd)_2$ to applied *P* using experimental Diamond Anvil Cell (DAC) studies and computational modeling techniques. The findings corroborated the previous literature[9,11] while also revealing the significance of ligand contribution to the conductive mechanism of this material to explain the discovered re-entrant insulator-to-metal-to-insulator transition.

In this work, we now present thin-oriented films that metalize under moderate pressure. To provide a more precise characterization of the material in its various forms and under different conditions, we have conducted both hydrostatic and uniaxial compression experiments on bulk powder pellets and thin films. Our research demonstrates the material's technological feasibility for uniaxial device operation and establishes its potential as a candidate PR material for the PET concept.[6,3,12] This extends the PET concept beyond the current paradigm of purely inorganic lanthanide PR materials, to also include the possibility of organic semiconductors and hence reveal the feasibility of an organic piezoelectronic transistor (OPET).

2. Experimental Section

2.1. Preparations and Forms

Details on the synthesis of $Pt(bqd)_2$ crystals are given in the previous work.[10] Crystals were then ground into fine particles using a pestle and mortar. Some of the resulting powder was compressed into pellets using a custom-made press for piston-cylinder cell (P-C cell) hydrostatic studies and another portion was deposited onto glass substrates using a physical vapor deposition system for uniaxial measurements.

2.2. Thin Film Deposition

Thin films of $Pt(bqd)_2$ (**Figure 3**) were deposited on a variety of substrates using a home-built physical vapor deposition system. Substrates used were: Fluorine-doped tin oxide (FTO), Kapton tape, plain glass, and gold-coated glass. The gold-coated glass was made by depositing a thin layer (≈2 nm) of Chromium onto the glass as an adhesion layer via electron-beam evaporation. Gold was then deposited on top using sputter coating. To form the contact for probing ρ, a mask was used to cover some area of the film during deposition (Figures S4,S5, Supporting Information).

2.3. Instrumentation

For the hydrostatic *P* studies, the large volume double layer P-C cell was developed (**Figure 4**).

P-C cell design specifications and materials can be found in Figure S6 (Supporting Information). This cell can reach a maximum *P* of 3 GPa and was particularly developed to contain bigger samples than a DAC, which in turn allows to more precisely allocate the *R* probing contacts and, therefore, to collect more accurate data. Another advantage of using the P-C cell over a DAC is improved hydrostaticity, such that the sample does not physically deform during an experiment. The feedthrough plug (Figures S6,S7, Supporting Information) allows in situ monitoring of the electronic behavior of the sample and Manganin wire (*P* manometer).

The uniaxial measurements were performed with the set-up shown in **Figure 5**.

The thin film was sandwiched between the flat surface of the stainless-steel C-clamp and the WC piston with a 600 µm cullet. The Force was applied with the hydraulic press and quantified with the spring with known stiffness by observing its displacement according to Equation (1). The spring was supported with spring stabilizers and friction between the piston & C-clamp and between the spring & spring stabilizers was minimized using MOLYKOTE grease as a lubricant.

$$F = -k \cdot x \quad (1)$$

where *F* is the force in N, *k* – spring stiffness, and *x* – displacement of the spring.

This measurement system allows precise quantification of *P* with small steps (≈7.6 MPa) and to collect data during *P* applications and releases.

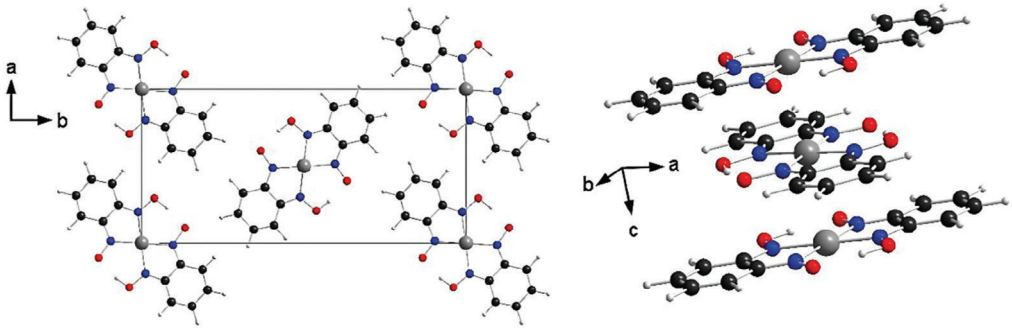

Figure 2. $Pt(bqd)_2$ crystal structure (space group *Ibam*). Atoms are colored: Pt (light grey), O (red), N (blue), C (dark grey), and H (white).

2.4. Resistivity in P-C Cell

The ρ studies in the P-C cell were performed on the compressed powder pellets. During pellet compression the sample molecules were randomly oriented within a finite pellet shape and, since $Pt(bqd)_2$ has an anisotropic nature, the most suitable technique for resistance (R) into ρ conversion was selected to be the Montgomery method.[13]

The probing contacts were bent onto a pellet (⌀ = 3 mm, thickness = 0.43 mm) with circumferential distribution and secured with silver paint and epoxy (Figure S8, Supporting Information). The resultant contact separation was then measured to be ≈1.433 mm (measured between silver epoxy boundaries).

High R measurements (> 2.1 MΩ) were performed using the *2-probe* method and a Keithley 6517A electrometer using the constant voltage method, and lower *Rs* were fulfilled using the *4-probe* method and a Keithley 2002 digital multimeter.

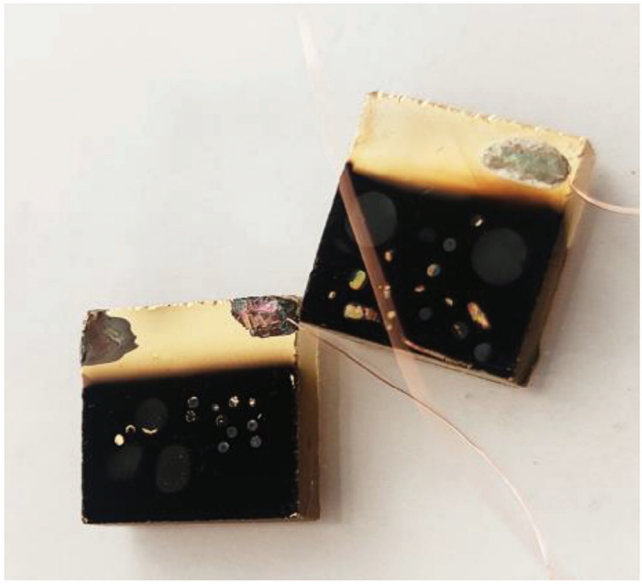

Figure 3. 10 mm x 10 mm $Pt(bqd)_2$ thin films (small circular patches are the points where load was applied).

2.5. Resistivity Measured under Uniaxial Load

The ρ studies in the uniaxial system were performed on the thin films (Figure 3) where $Pt(bqd)_2$ was grown on the substrate with the preferred needle orientation – aromatic molecules stacked along the *c-axis* (Figure 2).

The R was measured through the 4 μm thick layer of $Pt(bqd)_2$ using conventional Equation (2).

$$\rho = RA/t \tag{2}$$

where ρ is resistivity in Ωm, R is resistance, A is the cross-sectional area of the piston's cullet, and t is the thickness.

2.6. Temperature Analysis

The temperature (T)analysis was produced in the P-C cell studies with the help of the flexible resistive heaters of the polyimide type that were attached to the BeCu cylinder with thermally conductive tape. The sample T was assumed to be the same as the T of the BeCu cylinder's surface and was probed with a K-type thermocouple. The electric current source was used to control T in the resistive heaters.

Since the Manganin calibration of the $R - P$ scale requires *Ro* value at ambient P (Equation S1, Supporting Information), it was not possible to alter *Ts* during P application because the T changes at any given P affect R of the Manganin coil even with proper seasoning.[14,15] Instead, the constant T varying P method was employed, resulting in numerous experiments being produced.

2.7. Bandgap Calculation

The band gaps (BGs) were empirically derived from the plot of experimentally collected σ versus $1/T$ in accordance with Equation (3). The activation energy was assumed to = ½ BG[16] since there was no doping present in the sample material.

$$Ea = [(\Delta \mathrm{In} \cdot \sigma)/(\Delta 1/T)] \cdot k_b \tag{3}$$

where Ea – activation energy in eV, σ is conductivity, T – the temperature in K, and k_b – Boltzmann constant in eV/K.

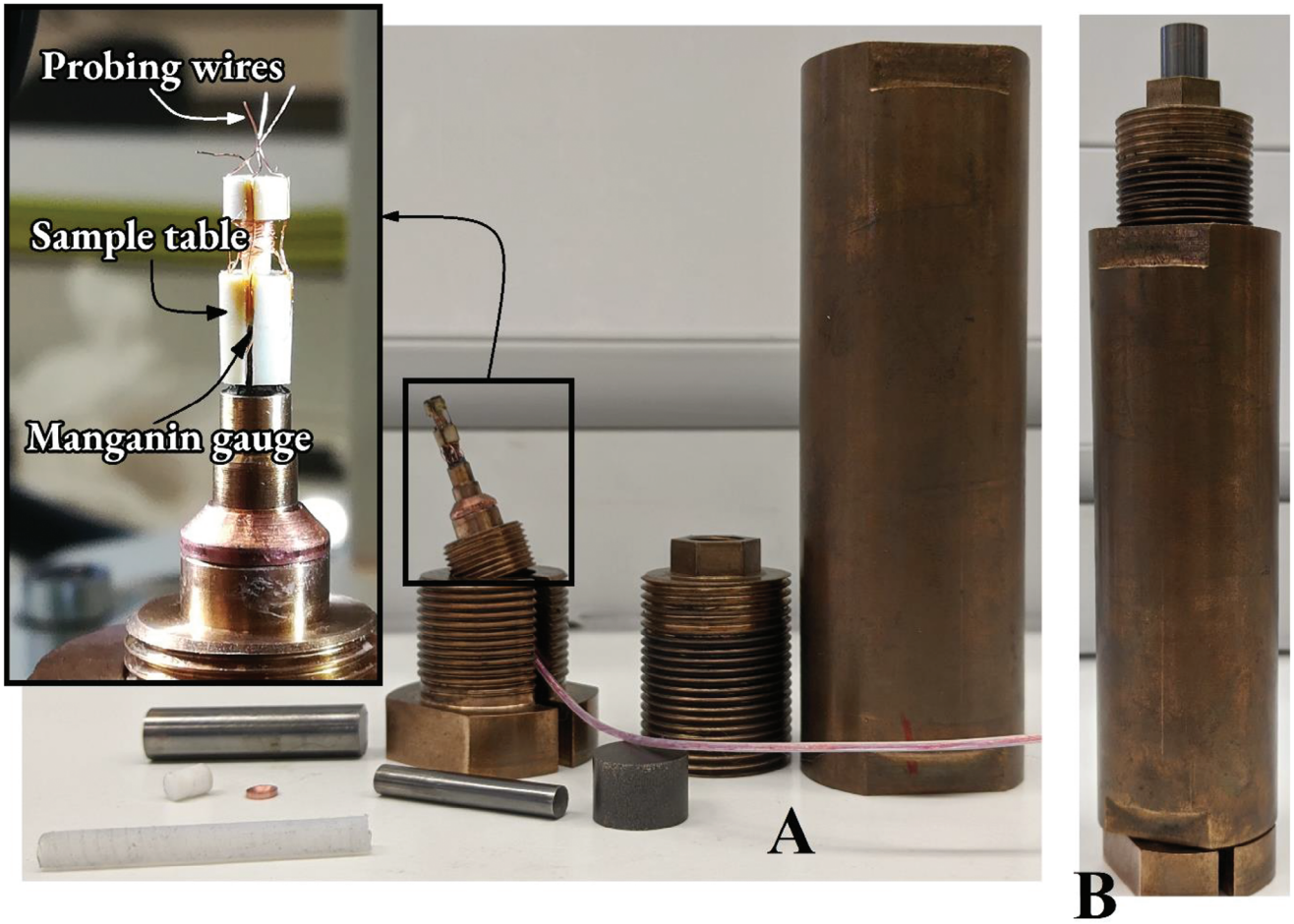

Figure 4. P-C cell with A – disassembled and B – assembled configuration. The zoomed-in insert (left) illustrates the feedthrough plug with a sample table.

3. Results and Discussion

3.1. Oriented Thin Films

Thin films of $Pt(bqd)_2$ complex were deposited on a variety of substrates using a home-built physical vapor deposition system (Figure S2, Supporting Information). $Pt(bqd)_2$ showed a strong degree of preferred orientation depending on the choice of the substrate (**Figure 6**): films deposited on glass, Kapton film, or fluorine-doped tin-oxide were oriented with the *Pt–Pt* chain lying parallel to the substrate whereas films grown on gold showed a strong preference for orienting with the *Pt–Pt* chain (*c-axis*) grow-

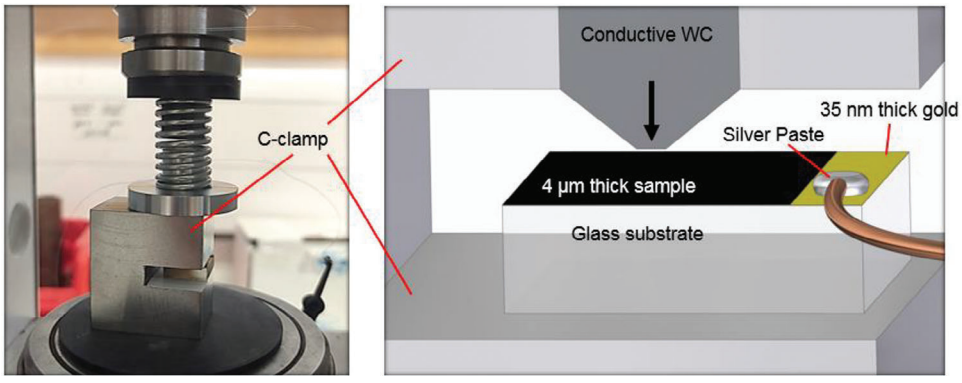

Figure 5. Uniaxial measurement set-up. Photo of the experimental set-up (left) and schematics of the experimental arrangement (right). The thickness of the sample at the maximum load used in the experiment was 4 μm.

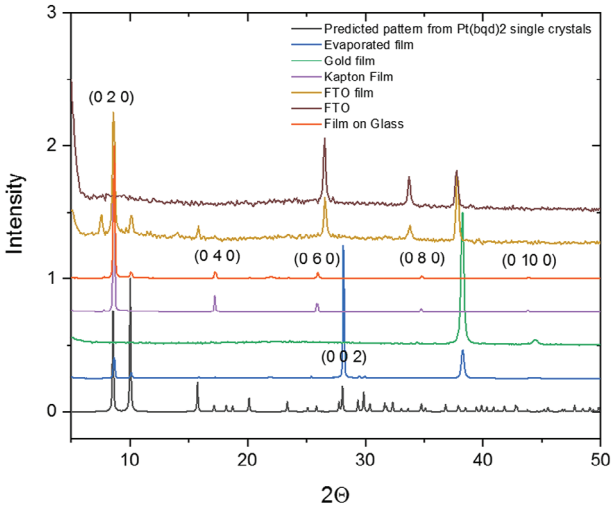

Figure 6. Powder diffraction patterns for $Pt(bqd)_2$ films deposited on a variety of substrates.

ing perpendicular to the substrate. As studies have shown that under *P* $Pt(bqd)_2$ shows the highest σ and greatest compressibility along the *c-axis*,[9,11,17] it was anticipated that this preferred orientation would be advantageous for constructing a thin film *P* responsive device (Figure 5). The orientated nature of the films on gold was confirmed by FIB-SEM measurements (**Figure 7**) which showed the film consisted of an array of vertically aligned needles; $Pt(bqd)_2$ is known to crystallise in the form of thin needles – with the *Pt-Pt* chain forming the needle axis.

The SEM images (Figure S10, Supporting Information) of the compression impact site showed after compression the average film height had decreased from ≈8 to ≈4 µm, which appeared to be due to the snapping of the crystalline needles. The cross-section of the impact site revealed that despite this compression the majority of the film still consisted of vertically oriented crystals. This was confirmed by powder X-ray diffraction data taken on a larger film that had been impacted (Figure S10, Supporting Information), which showed little change in orientational order after compression.

3.2. Compressed Powder P–ρ Studies

Figures 8 and **9** depict different experimental techniques and are accompanied by additional information such as computed BG, Pt-Pt distances, and structural parameters to facilitate analysis.

The electronic response of $Pt(bqd)_2$ compressed powder to the applied *P* obtained in the P-C cell was found to have an identical trend with that previously discovered in the DAC[10] with slightly higher ρ at elevated *P* (**Figure 8**). The exploitation of the P-C cell (Figure S6, Supporting Information) also allowed extensive *T* analysis on the sample by observing changes in sample ρ, *P*, and *T* in situ. The BG versus *P* relationship illustrated in Figure 8 was constructed using four *T* points: 293, 304, 313, and 324 K at selected points: 0, 0.2, 0.4, 0.6, 0.8, 1, 1.1, 1.2, 1.4, and 1.5 GPa.

Initially, BG decreases from ≈1.03 eV at ambient *P* with the computed value of *Pt-Pt* distance of 3.17 Å to ≈0.007 eV at 1.1 GPa where *Pt-Pt* distance decreases to 3.05 Å and the material reaches a metallic state. Although, the ρ was not increasing after 1.1 GPa (**Figure 9**), the experimentally derived BG values in the P-C cell fully agree with singe-crystal literature[9] and our computational work[10] where the material re-enters an insulator state at higher *P*.[9]

3.3. Thin Film P–ρ Studies

In contrast to the powder material (in which material grains are randomly oriented), we have observed extreme *P* sensitivity of electrical ρ in $Pt(bqd)_2$ (Figure 9) when it is deposited into thin film form with the preferred needle orientation perpendicular to the glass substrate (*Pt-Pt* atoms stack along *c-axis*).

The presence of both experimental and computational data enabled the generation of a comprehensive comparative analysis. Notably, crystallographic analysis[10] (Figure 9) illustrates that compressing the material along the *c-axis* reduces *Pt-Pt* distances, inducing a pronounced orbital overlap effect more than in any other dimension. This observation explains why uniaxial studies, when conducted along the preferred needle orientation, result in significantly lower metallization *P* compared to hydrostatically compressed powder studies.

The greatest change occurs between ambient *P* and only 100 MPa, where sample ρ drastically decreases from 120 kΩm to 60 Ωm (4 orders of magnitude change). Further *P* increases lead to comparatively moderate or 1 order of magnitude change in ρ. Although the load increase and decrease trends sometimes overlap due to the dynamic spring friction, they stay in close agreement and illustrate that sample ρ recovers to the original value at ambient pressure. Moreover, additional cycling of the same indentation areas further demonstrates the reversibility and repeatability of the ρ versus *P* data (Figure S11, Supporting Information).

This discovery illustrates that $Pt(bqd)_2$ requires a much lower metallization *P* than any PR candidates proposed so far for PET, which makes it an ideal candidate.

The presence of both experimental and computational data enabled the generation of a thorough comparative analysis and facilitated data discussion.

4. Conclusion

To summarise, herein we demonstrate a unique high-potential PR material candidate for the PET concept that was proposed by IBM.[2,3,12] $Pt(bqd)_2$ can be readily synthesized and grown on the gold-coated substrate with the required thickness by controlling the loading amount in the deposition system. Highly crystalline-oriented films form needle-like structures and provide highly sensitive conductive pathway under the influence of comparatively very low uniaxial *P*. The thin film studies illustrate a massive 4-order of magnitude change in ρ under just 100 MPa of uniaxial *P*. The extreme *P* dependence of the electronic properties is due to the high crystal structure compressibility of $Pt(bqd)_2$ intramolecular interactions, which are weak and do not lead to high intermolecular repulsion when molecules are pressed closer. Further cycling (Figure S11, Supporting Information) confirms the

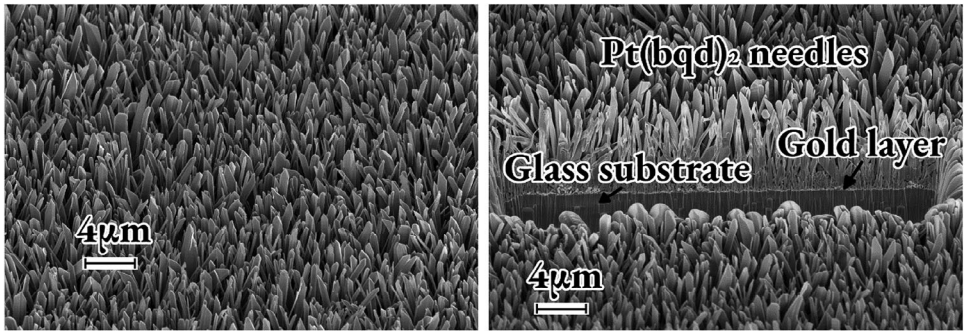

Figure 7. SEM images of $Pt(bqd)_2$ film deposited on a gold-coated glass substrate (the patch was made with FIB to evaluate the thickness of the film).

trend illustrated in Figure 9, confirming the material's potential as a PR candidate. It is important to note that our primary objective was to establish a proof of concept for $Pt(bqd)_2$'s remarkable properties. While we have not pursued the development of a functional device in this study, the promising results open new avenues for further research and practical applications.

Compared to the other, so far proposed PRs, $Pt(bqd)_2$ is reasonable in terms of price and abundance and nonreactive with air or other PET components (SmSe is chemically incompatible with PE and oxidizes in the air).[6] Moreover, organic electronic materials are highly tuneable through synthetic modification, as has been much illustrated in the optimization of materials for, that is, organic FETs (OFET)[18] or organic photovoltaics (OPV).[19] This first demonstration of organic material with appropriate thin-film pressure-conductivity behavior for the PET opens up space for synthetic modifications and new molecular designs to further develop and optimize new OPET materials. In particular, the extremely low metallization P of oriented $Pt(bqd)_2$ indicates that much smaller PE energy efforts are required for device switching, with opportunities for modification and choice of other device components.

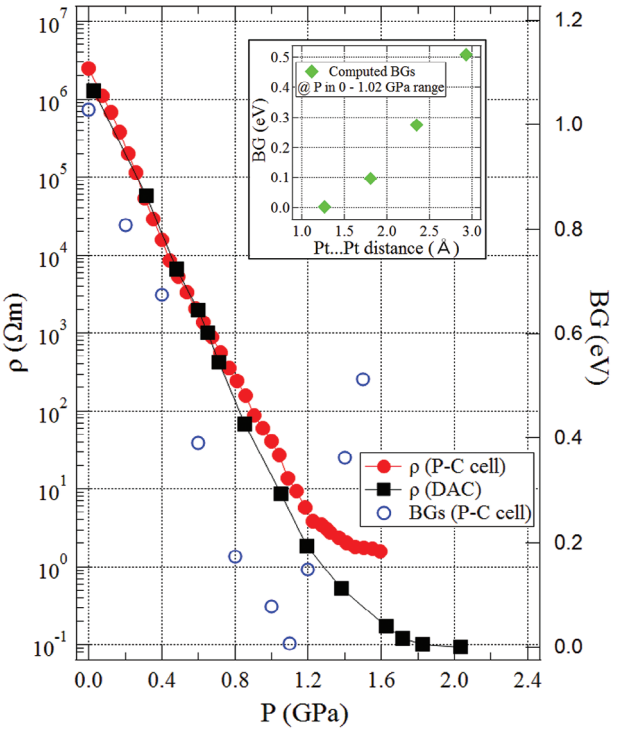

Figure 8. Compressed powder $Pt(bqd)_2$ studies in DAC and P-C cell. Empirical BGs were derived from P-C cell T studies. The insert shows computed BG versus *Pt–Pt* distances.

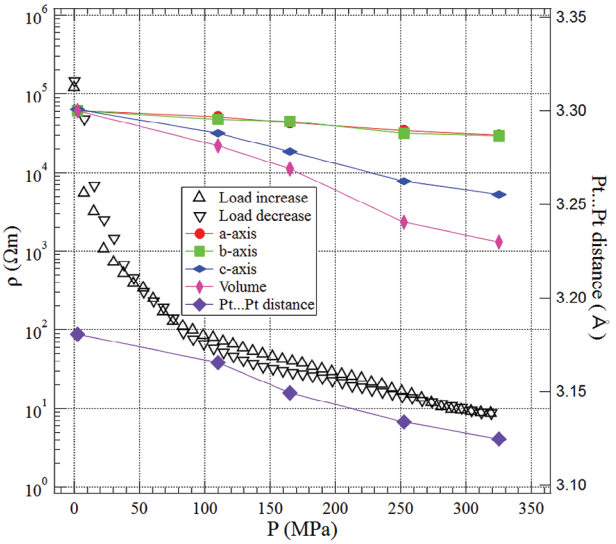

Figure 9. Pressure dependence of thin film $Pt(bqd)_2$ electrical resistivity (left axis) compared to structural parameters (right axis).

Supporting Information

Supporting Information is available from the Wiley Online Library or from the author.

Acknowledgements

We gratefully acknowledge the Leverhulme Trust (RPG-2016-152) for funding support. Special thanks to Mr. David McCabe for his valuable contributions in fabricating the instrumentation components. We also acknowledge the valuable insights and early-stage discussions provided by Glenn Martyna and Dennis Newns on the device context.

Conflict of Interest

The authors declare no conflict of interest.

Data Availability Statement

The data that support the findings of this study are available from the corresponding author upon reasonable request.

Keywords

conductivity, organic, piezoelectronic, pressure, Transistor

Received: October 3, 2023
Revised: December 19, 2023
Published online:

[1] M. M. Waldrop, *Nature* **2016**, *530*, 144.
[2] B. Elmegreen, et al., 4-terminal piezoelectronic transistor, US patent application YOR920110425US1, **2014**.
[3] D. M. Newns, B. G. Elmegreen, X.-H. Liu, G. J. Martyna, *MRS Bull.* **2012**, *37*, 1071.
[4] M. Copel, M. A. Kuroda, M. S. Gordon, X.-H. Liu, S. S. Mahajan, G. J. Martyna, N. Moumen, C. Armstrong, S. M. Rossnagel, T. M. Shaw, P. M. Solomon, T. N. Theis, J. J. Yurkas, Y. Zhu, D. M. Newns, *Nano Lett.* **2013**, *13*, 4650.
[5] Y. Shirota, H. Kageyama, *Chem. Rev.* **2007**, *107*, 953.
[6] J. B. Chang, H. Miyazoe, M. Copel, P. M. Solomon, X.-H. Liu, T. M. Shaw, A. G. Schrott, L. M. Gignac, G. J. Martyna, D. M. Newns, *Nanotechnology* **2015**, *26*, 375201.
[7] J. M. Williams, J. R. Ferraro, R. J. Thorn, *Organic Superconductors (Including Fullerenes): Synthesis, Structure, Properties, and Theory*, Prentice Hall, Hoboken **1992**.
[8] B. M. Anderson, S. K. Hurst, *Eur. J. Inorg. Chem.* **2009**, *21*, 3041.
[9] K. Takeda, I. Shirotani, C. Sekine, K. Yakushi, *J Phys Condens Matter* **2000**, *12*, L483.
[10] H. Benjamin, J. G. Richardson, S. A. Moggach, S. Afanasjevs, L. Warren, M. R. Warren, D. R. Allan, C. A. Morrison, K. V. Kamenev, N. Robertson, *Phys. Chem. Chem. Phys.* **2020**, *22*, 6677.
[11] I. Shirotani, A. Kawamura, K. Suzuki, W. Utsumi, T. Yagi, *Bull. Chem. Soc. Jpn.* **1991**, *64*, 1607.
[12] D. M. Newns, B. G. Elmegreen, X.-H. Liu, G. J. Martyna, *Adv. mater.* **2012**, *24*, 3672.
[13] H. C. Montgomery, *J. Appl. Phys.* **1971**, *42*, 2971.
[14] L. H. Dmowski, E. Litwin-Staszewska, *Meas. Sci. Technol.* **1999**, *10*, 343.
[15] G. Yiannakopoulos, *A Review of Manganin Gauge Technology for Measurements in the Gigapascal Range*, DSTO Materials Research Laboratory, Maribyrnong **1990**.
[16] S. M. Sze, K. K. Ng, *Semiconductor Devices Physics and Technology*, 3rd ed., John Wiley & Sons, Hoboken **2007**.
[17] K. Takeda, I. Shirotani, K. Yakushi, *Synth. Met.* **2003**, *133*, 415.
[18] A. K. Chauhan, P. Jha, D. K. Aswal, J. V. Yakhmi, *J. Electron. Mater.* **2022**, *51*, 447.
[19] F. Zhao, J. Zhou, D. He, C. Wang, Y. Lin, *J. Mater. Chem. C.* **2021**, *9*, 15395.